DOI:
10.1088/1361-6668/ad9864

Document Version
Peer reviewed version

Comparison of J_c measurements obtained by magnetisation and transport methods for a GdBCO-Ag bulk

R. W. Taylor[1,2], A. E. Pantoja[1], S. V. Chong[1,2], T. Hlásek[3,4], J. Plecháček[3], H. W. Weijers[1], M. D. Ainslie[5], R. A. Badcock[1,6] and C. W. Bumby[1,2]

[1]Paihau-Robinson Research Institute, Victoria University of Wellington, Wellington, New Zealand
[2]The MacDiarmid Institute for Advanced Materials and Nanotechnology, Wellington, New Zealand
[3]CAN SUPERCONDUCTORS s.r.o, Kamenice, Czech Republic
[4]Department of Inorganic Chemistry, University of Chemistry and Technology Prague, Prague, Czech Republic
[5]Department of Engineering, King's College London, London, United Kingdom
[6]Te Whai Ao - Dodd-Walls Centre for Photonic and Quantum Technologies, University of Otago, Dunedin, New Zealand

E-mail: ross.taylor@vuw.ac.nz; chris.bumby@vuw.ac.nz

September 2024

Abstract.

Accurate numerical modelling of bulk rare-earth barium cuprate ((RE)BCO) high-temperature superconductors requires measured data of the temperature and magnetic field dependence of the critical current density, J_c, and flux-flow exponent, n. However, there is limited published J_c and n data for modern (RE)BCO bulks. In this work, transport and magnetisation methods were applied to characterise J_c, n, and the critical temperature, T_c, of a commercially available top-seeded melt growth (TSMG) GdBCO-Ag bulk. Both measurement methods exhibit good quantitative and qualitative agreement when the transport electric field criterion is scaled from 1 μV/cm to 10^{-4} μV/cm.

Transport-derived thermo-magneto-angular dependent J_c data for the TSMG GdBCO-Ag bulk are compared to equivalent data for a SuNAM SCN12700 GdBCO coated-conductor tape. Significant qualitative differences are observed between the data for the bulk and tape, with the tape data featuring neither a fishtail effect nor a $B \parallel c$ peak, both of which are present in the bulk data.

A reliable sample preparation and mounting method is presented, which enables the transport characterisation of (RE)BCO bulk superconductors over a large range of temperatures and applied field magnitudes and angles.

All J_c and n data presented within this manuscript are available in the *Supplementary Material*, and can be interpolated into finite-element models to more accurately capture the superconducting behaviour of GdBCO superconductors.

1. Introduction

Bulk rare-earth barium cuprate ((RE)BCO) high-temperature superconductors (HTS) are used in applications such as magnetic levitation, bearings, quasi-permanent magnets, undulators, NMR and MRI [1–9]. Numerical simulations enable rapid and cost-effective design iteration of such devices, but require accurate data of the critical current density, J_c, and flux-flow exponent, n, of the superconductor over a wide range of conditions [10].

Magnetisation techniques are the most popular method to determine J_c for small samples of bulk superconductor. This is due to the simplicity of the required sample preparation and wide availability of the instrumentation. Many (RE)BCO systems have been characterised using this approach, including YBCO, GdBCO, EuBCO, and others [11–21]. However, the values of J_c obtained through this method are calculated indirectly using the extended Bean model [22], and assume a uniform distribution of J_c throughout the small sample. Consequently, this approach struggles to distinguish inhomogeneities caused by microstructural variations or magneto-angular anisotropy. Furthermore, (RE)BCO materials typically exhibit highly anisotropic superconducting properties due to their layered, oxygen-deficient perovskite structures [23, 24]. Magnetisation measurements of n-value are challenging, as they require transient magnetic relaxation measurements [25–27], which are often dominated by the inductance of the measurement coils themselves. As a result, there is a dearth of published n-value data for these materials.

An alternative method to characterise J_c and n-value in bulk superconductors is through a four-point transport current measurement, which is the standard approach for characterising wire-based superconductors. In this approach, the voltage across a sample is measured whilst a current is applied. The resulting voltage response is fitted to the E-J power law [28, 29], where J is equal to the applied current divided by the cross-sectional area of the measured sample. Both J_c and n-value are obtained as fitting parameters. In transport measurements, there is a defined current axis. This enables full resolution of the thermo-magneto-angular anisotropy of J_c and n-value in the measured sample, $J_c(T, B, \theta)$ and $n(T, B, \theta)$.

Transport measurements on HTS bulks are not commonly reported, as they require specialist equipment and thin sample cross-sections to enable access to I_c using standard power supplies. Preparing such samples without material damage is challenging due to the brittle nature of (RE)BCO bulks [30]. Previous work has been predominantly focussed on the self-field case for YBCO at 77 K (liquid N_2) [11, 31–37], but more recent efforts have studied other bulks such as DyBCO, (NdEuGd)BCO and GdBCO-Ag [17, 20, 21, 38, 39].

This work reports the superconducting properties of a top-seeded melt growth (TSMG) GdBCO-Ag bulk, with a comparison of results obtained from transport and magnetisation characterisation methods. Additionally, the transport $J_c(T, B, \theta)$ behaviour is compared with that of an HTS GdBCO coated conductor tape. These measurements were achieved through development of the sample preparation and mounting methods presented in [39]. The measured J_c and n-value data are presented in a manner that can be directly interpolated into numerical models [40], and all data contained within this manuscript are available in the *Supplementary Material*.

2. Methodology

2.1. Sample preparation

A commercially available 35 mm diameter, 10 mm thick single-grain GdBCO-Ag bulk (CAN Superconductors) was used in this work. This was prepared by the buffer-assisted TSMG technique from a precursor powder with nominal composition $Gd_{1.8}Ba_{2.45}Cu_{3.4}O_x$ + 10 w.t.% Ag_2O [41]. A 2 mm × 2 mm NdBCO thin film on an MgO substrate was used as a seed, with an 8 mm diameter, 1.5 mm thick buffer pellet from the same precursor powder used to promote c-sector growth. The grown bulk was then annealed in flowing O_2 (360-400°C, 2 weeks). Figure 1 shows a typical cross-section of a buffer-assisted TSMG bulk.

The GdBCO-Ag bulk was cut parallel to the a-b plane into ≈0.8 mm thick wafers using a diamond wire saw. The wafer surfaces were polished using P2500 (8.4 µm particle) SiC paper to ensure a flat finish and remove areas of edge damage. Rectangular bars of width ≈2 mm were then cut from the wafers (Fig. 2a).

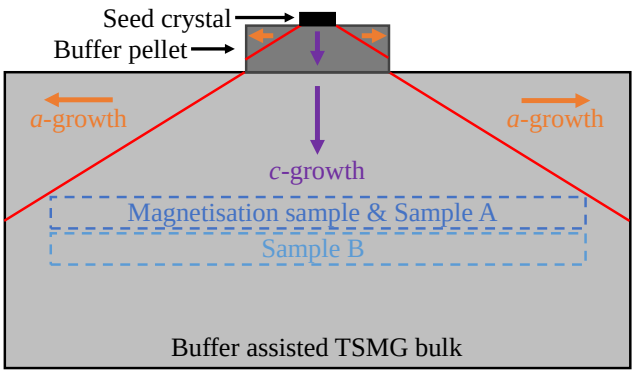

Figure 1. Typical cross-section of a buffer-assisted TSMG bulk, with crystallographic growth direction shown. The blue dashed boxes indicate the cut locations of the samples discussed in this manuscript.

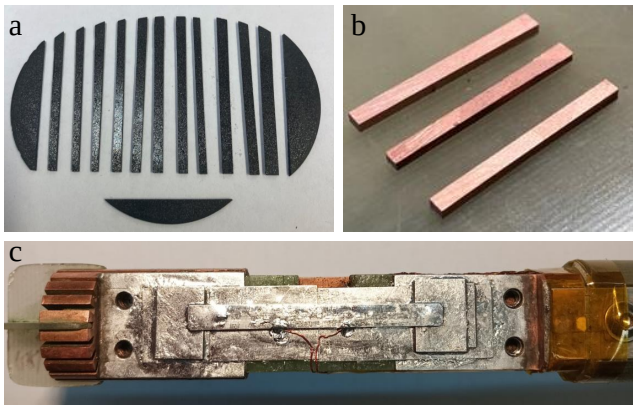

Figure 2. (a) Bars cut from a TSMG GdBCO-Ag wafer. (b) TSMG GdBCO-Ag bars coated in ≈20 µm of Ag and ≈20 µm of Cu. (c) TSMG GdBCO-Ag bar mounted on the SuperCurrent probe. The bar is soldered onto two Cu sheets, with a brass piece soldered on top for mechanical and thermal reinforcement.

Magnetisation measurements were made on a 1.15 × 2.27 × 0.84 mm^3 cuboidal sample cut from the centre of a bar taken from a wafer that was ≈4 mm below the seed crystal.

In order to make transport measurements, an ≈20µm thick layer of silver was evaporated onto the bars, which were then annealed in an oxygen environment at 450°C for 1 h. An ≈20µm thick layer of copper was then evaporated onto the bars (Figure 2b). The entire bar was then tinned using In-Bi solder. A piece of Cu sheet was soldered onto each of the main Cu terminals on the sample probe with In-Ag solder, in order to increase the electrical contact area and therefore lower the resistance and heating. The GdBCO-Ag bar was then soldered onto the Cu sheets, and voltage taps were soldered onto the side of the GdBCO-Ag bar. To provide thermal and mechanical reinforcement, a brass piece was soldered on top of the GdBCO-Ag. The final assembly is shown in Figure 2c. This sample preparation and mounting method is based on that reported in [39], with minor adaptations which have increased the measurable current limit from 400 A to 1.2 kA and prevented sample failure during cooling, which previously occurred in ≈40% of samples.

Data for two TSMG GdBCO-Ag samples are reported in this work. Sample A was a 1.83 × 30 × 0.79 mm^3 bar cut from a wafer ≈5 mm below the seed crystal and prepared using the above method. Sample B was a 1.59 × 30 × 0.58 mm^3 bar cut directly adjacent to and from the same wafer as the magnetisation sample. Some data for Sample B has been previously reported in [39].

All bulk samples discussed in this manuscript were cut from within regions in the c-growth sector.

2.2. Magnetisation measurements of T_c and J_c

The cuboidal GdBCO-Ag sample was measured using a Quantum Design MPMS XL SQUID Magnetometer.

To measure the critical temperature, T_c, the sample was zero-field cooled to 70 K before a 1 mT field was applied parallel to the c-axis. The sample temperature was then increased at 1.5 K/min to 100 K, and T_c was obtained by observing the onset of sample demagnetisation. The value of T_c was determined as the temperature at which the magnetic moment of the sample reduced to 90% of its original value.

Field sweeps were performed to measure m-H hysteresis loops, and J_c (in A/m^2) was calculated from experimental data with the following equation, based on the extended Bean model [22]:

$$J_c(H) = \frac{2 \times 10^5 \cdot \Delta m(H)}{a\left(1 - \frac{a}{3b}\right) abc}, \qquad (1)$$

where $\Delta m(H) = m(H)^+ - m(H)^-$ is the height of the hysteresis loop (in emu), a and b are the shortest and longest side lengths in the a-b plane respectively (in cm) and c is the thickness parallel to the c-axis (in cm).

2.3. Transport measurements of T_c, I_c and n

Transport measurements were made using the SuperCurrent system, which employs an HTS magnet and rotating sample probe to measure I_c and n for transport currents of up to 1.2 kA, at $B \leq 8$ T, $\theta = -360°$ to $+360°$ and $T \geq 15$ K [42,43]. Here θ represents the angle that the applied field makes to the c-axis of the sample. The system has previously been used extensively to characterise coated-conductor HTS tapes [44–50] and BSCCO wires [51].

The critical temperature is measured in the SuperCurrent system by zero-field cooling the sample and then applying a 10 mA direct current whilst gradually heating the sample at 1 K/min until it reaches the superconducting transition. The value of T_c was determined as the temperature at which V reached 10% of the maximum value, in a manner analogous to the magnetisation method criteria.

The critical current, I_c, is defined as the current at which the measured voltage corresponds to a threshold electric field, E_c. Typically, $E_c = 1$ µV/cm is chosen, and this value is used throughout this work unless stated otherwise. Values of I_c and the flux-flow exponent n are calculated by fitting the $V(I)$ dependence to

$$V = V_c \left(\frac{I}{I_c}\right)^n + V_0 + R_1 I, \qquad (2)$$

where $V_c = d \cdot E_c$, d is the distance between voltage taps, V_0 is the instrumental zero offset and R_1 accounts

for dynamic and contact resistances. Division of I_c by the cross-sectional area of the sample yields J_c.

3. Results and Discussion

3.1. T_c results

Temperature sweep magnetisation data and transport data for Sample A are presented in Figure 3. The magnetisation- and transport-derived T_c values are ≈93.6 K and 93.8 K respectively, consistent both with each other and the expected values from the literature for TSMG GdBCO-Ag [15]. Note that a much higher data density is possible in transport measurements than in magnetisation measurements, because the acquisition time is significantly faster (20 ms versus 15 s).

3.2. Self-field temperature dependencies of J_c and n

The self-field temperature dependencies of critical current density and n-value, $J_c(T, 0\ \mathrm{T})$ and $n(T, 0\ \mathrm{T})$ respectively, for Sample A are shown in Figure 4. Magnetisation-derived $J_c(T, 0\ \mathrm{T})$ results are also plotted for comparison. In both the transport and magnetisation results, $J_c(T, 0\ \mathrm{T})$ increases monotonically and approximately linearly as T decreases. There is close agreement of $J_c(T, 0\ \mathrm{T})$ between methods for $T \geq 80$ K, but at lower temperatures these values start to diverge, with the transport-derived $J_c(T, 0\ \mathrm{T})$ consistently larger. The n-values rise rapidly with falling temperature near T_c (where $n = 1$), before plateauing at $n \approx 18$.

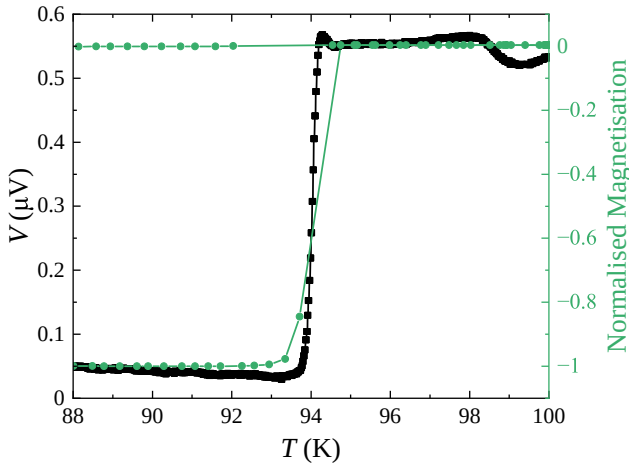

Figure 3. Temperature dependence of measured voltage with $I = 10$ mA and normalised magnetisation from an equivalent magnetisation measurement with an applied field of 1 mT for a TSMG GdBCO-Ag bulk. Transport data is shown for Sample A.

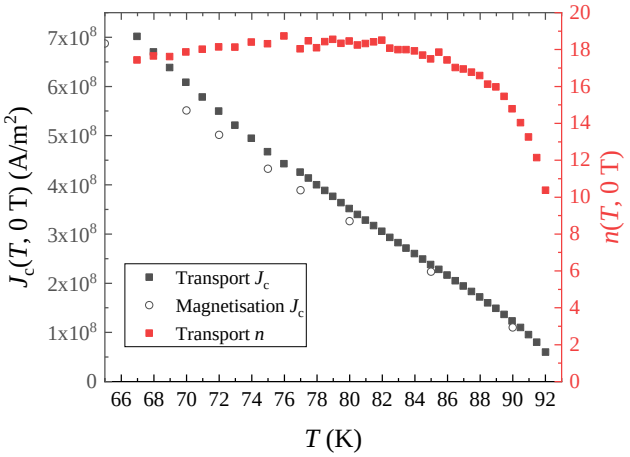

Figure 4. Self-field temperature dependence of J_c and n for a TSMG GdBCO-Ag bulk. Transport data is shown for Sample A.

3.3. In-field temperature dependencies of J_c and n

The magnetic field dependence of J_c for a field applied parallel to the c-axis of a TSMG GdBCO-Ag sample, $J_c(T, B_\perp)$, is shown for the magnetisation data and for transport Sample A in Figures 5a and 5b, respectively.

The $J_c(T, B_\perp)$ behaviour is qualitatively similar for both the magnetisation- and transport-derived results. At all temperatures there is an initial exponential decrease in J_c at low applied fields, typically attributed to δl-pinning, caused by the presence of non-superconducting defects (such as from vortices, oxygen vacancies, impurities, grain boundaries and irradiation) causing spatial variations in the electron mean free path l [52–55]. As the temperature decreases, a second peak emerges at high fields resulting in a 'fishtail' effect. A variety of phenomena have been identified as potential causes of the fishtail effect [52–65], however, the second peak in (RE)BCO bulks is generally attributed to δT_c-pinning. The δT_c-pinning arises from localised clusters of material with poorer superconducting properties, typically oxygen-deficient (RE)$Ba_2Cu_3O_{7-\delta}$ phase [52–58], scattered throughout the bulk. The weak pinning in these clusters strengthens as the applied field increases, until it reaches a maximum value when the low-T_c clusters become normal. As the applied field increases beyond this point, vortices cannot be pinned as effectively and J_c decreases. The fishtail effect has previously been observed in the $J_c(T, B_\perp)$ data of many bulk (RE)BCO samples calculated using both magnetisation and transport techniques [56, 66–68], including for GdBCO-Ag [14, 39].

The transport-derived in-field dependence of n, $n(T, B_\perp)$, is shown for Sample A in Figure 5c. The fishtail effect is present in the n data, and is significantly more pronounced than in the J_c data.

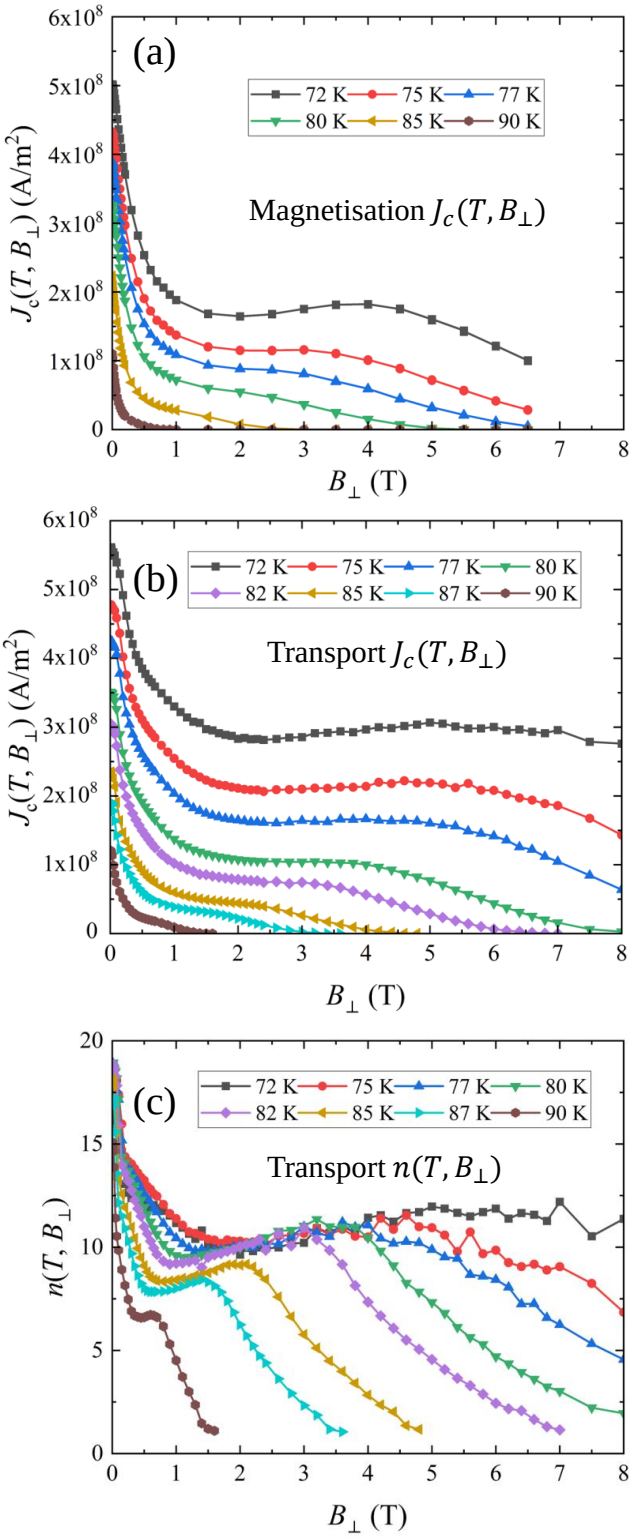

Figure 5. Magnetic field dependence of J_c and n for a field applied parallel to the c-axis of a TSMG GdBCO-Ag bulk. (a) Magnetisation-derived $J_c(T, B_\perp)$ data, (b) Transport-derived $J_c(T, B_\perp)$ data for Sample A, (c) Transport-derived $n(T, B_\perp)$ data for Sample A.

The measured n-value is highly field and temperature dependent, and does not exceed 19 in the measured T range. Numerical simulations of TSMG GdBCO-Ag bulks typically assume a constant value of $n = 20$ and focus on applications with $B > 1$ T [14, 69–71]. An unrealistically high and constant n-value could lead to significant differences between simulation and experiment.

3.4. Transport and magnetisation result comparison

Both the magnetisation sample and transport Sample B were cut from the centre of the same wafer. The samples were cut adjacent to each other, which allows for a direct comparison of the $J_c(T, B_\perp)$ results obtained using each method for samples with similar microstructure. The transport and magnetisation $J_c(T, B_\perp)$ data are shown in Figure 6a.

The measured transport J_c is significantly higher than the magnetisation value at all measured temperature and applied field combinations. This is because magnetic measurements are more susceptible to flux creep than transport measurements [72]. As a result, there is a difference in the effective electric field criterion in each case. The transport method applies a driving voltage equivalent to a threshold value of 1 µV/cm. This ensures that unidirectional currents are flowing throughout the sample, and experiencing a dissipative resistance throughout.

However, this is not the case for the magnetisation method. Instead, these measurements are made once the magnetising currents circulating within the sample have stabilised through relaxing into the non-dissipative regime (at least on the timescale of the experiment). As such, the equivalent 'effective threshold field' from Equation 2 is much smaller for magnetisation measurements than the value utilised for transport measurements. For (RE)BCO materials, this is typically found to be within the range $10^{-8} - 10^{-3}$ µV/cm [73].

Magnetisation relaxation due to flux creep is complex to describe mathematically, as it depends on temperature, applied field, sample geometry and other material property effects. However, a useful correction factor can be obtained through simply assuming a different constant electric field criterion for each method.

In order to better compare the two methods, the transport data was refit to Equation 2 with all parameters kept the same except E_c and I_c. The transport J_c with $E_c = 10^{-4}$ µV/cm is compared to the magnetisation data in Figure 6b. This shows that the simple transformation of the critical electric field criterion is sufficient to deliver good qualitative and quantitative agreement between the methods.

Note that there is some variation in the $J_c(T, B_\perp)$

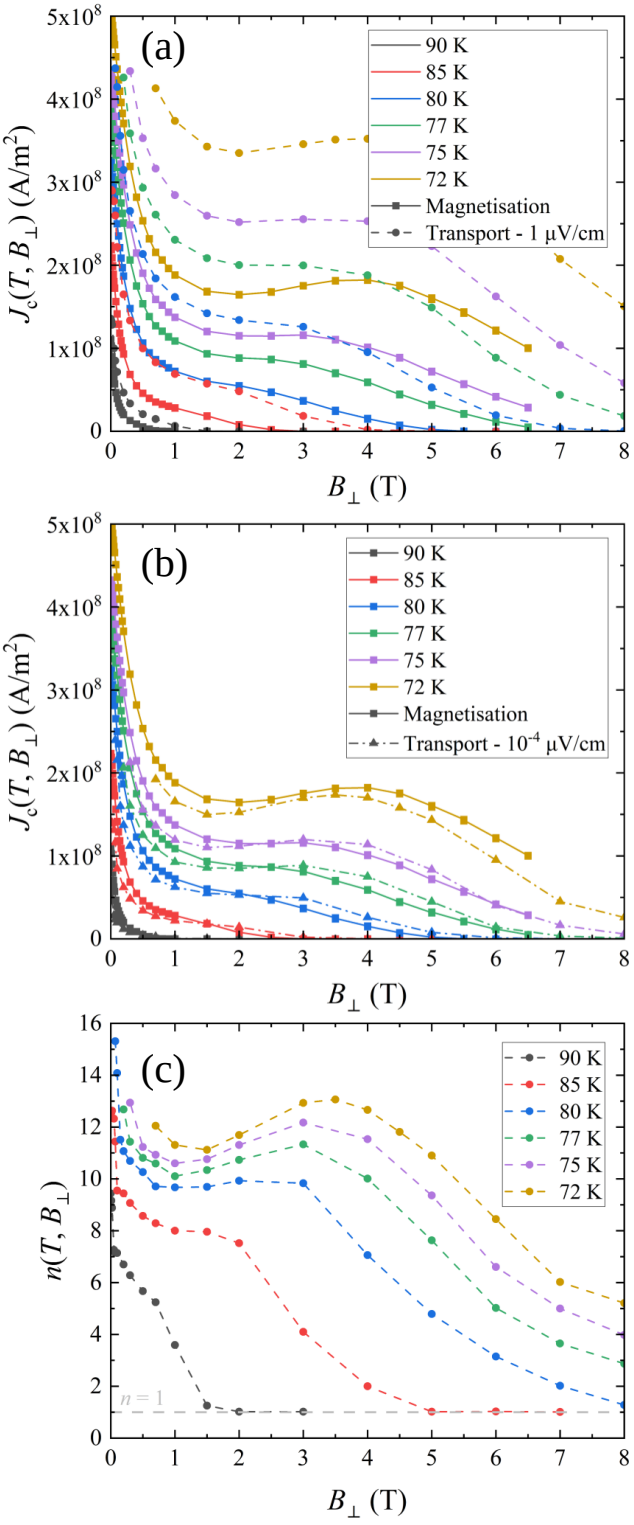

Figure 6. Field dependence of J_c characterised using both transport and magnetisation methods for a TSMG GdBCO-Ag bulk. (a) Transport electric field criterion $E_c = 1$ μV/cm. (b) Transport electric field criterion $E_c = 10^{-4}$ μV/cm. (c) Transport $n(T, B_\perp)$ data. Transport data is shown for Sample B.

data measured for transport Samples A and B, which is likely caused by the pieces being cut from a different location relative to the seed crystal. Variation of J_c within a TSMG GdBCO bulk has been previously observed and studied in detail using magnetisation techniques in [15,16], and was linked to microstructural inhomogeneities throughout the bulk.

A threshold of $E_c = 1$ μV/cm is used in the transport results from hereon, as this is the typical value used when modelling HTS bulks.

3.5. $J_c(T, B, \theta)$ and $n(T, B, \theta)$ Results

Measured $J_c(77\text{ K}, B, \theta)$ and $n(77\text{ K}, B, \theta)$ data for Sample A are shown in Figure 7a. Here θ is the angle of the applied B-field relative to the c-axis, i.e. $\theta = 0°$ corresponds to $B \parallel c$ and $\theta = 90°$ corresponds to $B \parallel a/b$. There is a strong angular dependence in both J_c and n, particularly around the 90° peak. Additionally, the $n(77\text{ K}, B, \theta)$ data broadly resemble the $J_c(77\text{ K}, B, \theta)$ data. Local maxima in both J_c and n are observed when B is parallel to both the crystallographic a-b plane and c-axis.

An angle-dependent fishtail effect is present in the $J_c(77\text{ K}, B, \theta)$ data, and can be observed by considering how J_c varies with B along lines of constant θ. For example, at $\theta = 10°$, J_c decreases monotonically until 1.5 T, and then starts to increase until 5 T before decreasing again. A simple indicator of the fishtail effect in this data is that the lines representing different field magnitudes cross. There is a significant depression of J_c at 8 T, however, the measured I-V curve still exhibits non-linear behaviour ($n > 1$) characteristic of the superconducting flux-flow regime.

For comparison, Figure 7b shows $J_c(77.5\text{ K}, B, \theta)$ and $n(77.5\text{ K}, B, \theta)$ data for a 12 mm wide Cu-plated SuNAM SCN12700 GdBCO coated-conductor tape using data from [74]. Both the critical current density and the n-value are significantly higher in the tape, with the self-field values of both materials shown in Table 1.

There are prominent qualitative differences between the $J_c(B, \theta)$ and $n(B, \theta)$ data of the GdBCO tape and bulk, with the SuNAM tape exhibiting a less complex angular dependence. Unlike the bulk, the tape does not exhibit the fishtail effect with increasing $|B|$. Instead both J_c and n decrease monotonically with $|B|$ for any given θ. As the effect is attributed to spatial variation of T_c, this is likely because the tape growth-process is more controlled and the resultant thin films are of higher quality. Additionally, the drastically higher aspect ratio in coated conductors ensures all material has the same oxygen doping, whereas the doping in bulks can vary due to the low oxygen diffusion coefficients of (RE)BCO materials and relatively large diffusion length scales. Another qualitative difference is that there are local maxima located

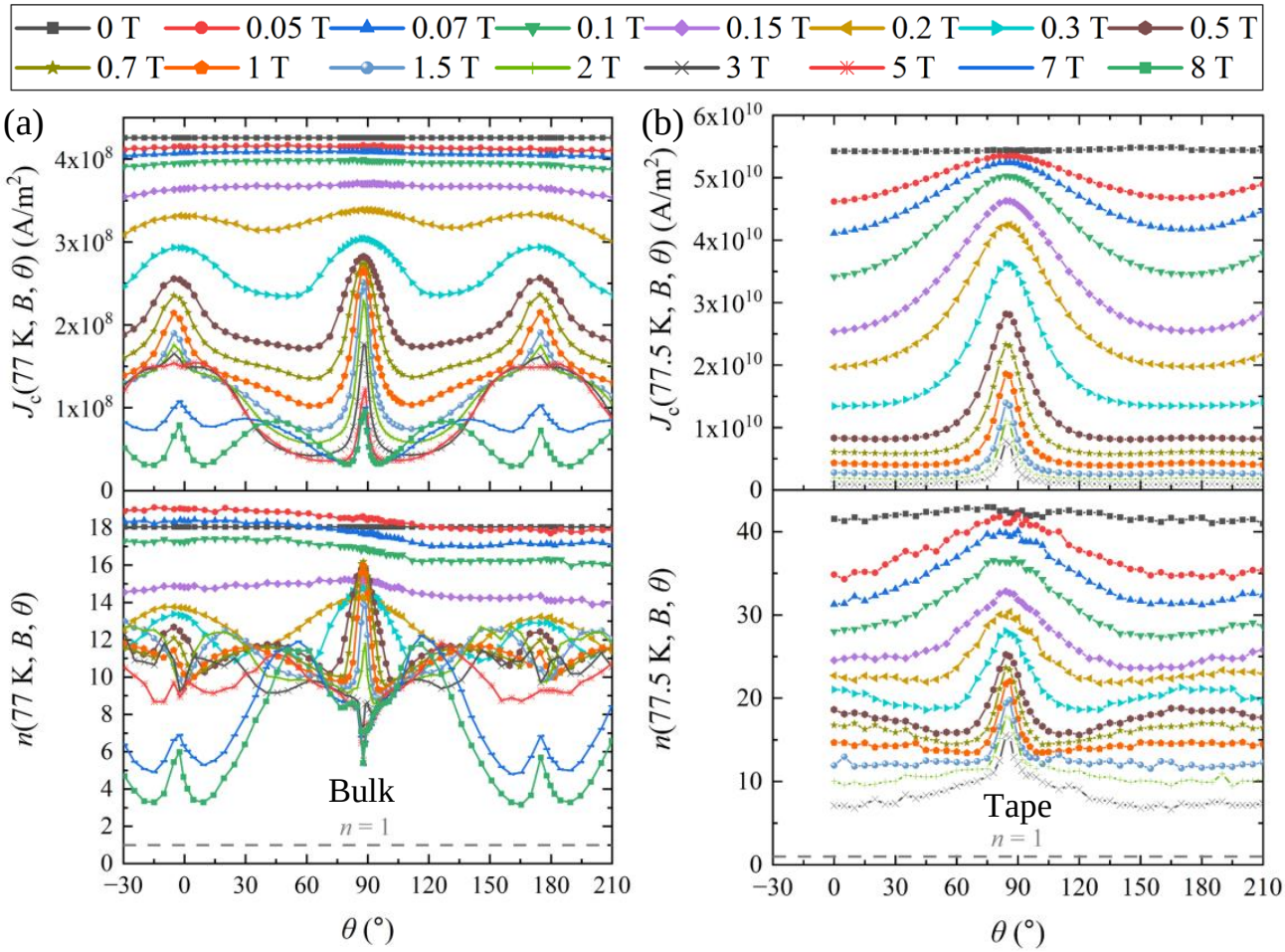

Figure 7. Measured $J_c(B,\theta)$ (top) and $n(B,\theta)$ (bottom) for: (a) Bulk TSMG GdBCO-Ag Sample A at 77 K and (b) A 12 mm wide copper-plated SuNAM SCN12700 GdBCO coated-conductor tape at 77.5 K, data from [74]. An additional dataset for the tape is included in the *Supplementary Material*, where the data has been corrected for self-field effects using the technique presented in [75], and the $n(B,\theta)$ data has been smoothed using the Savitzky-Golay method to improve numerical convergence.

at $B \parallel c$ ($\theta = 0°$ or 180°) in the $J_c(B,\theta)$ and $n(B,\theta)$ data for the bulk, but not the tape. The $B \parallel a/b$ peak in the $J_c(B,\theta)$ data is caused by a mixture of intrinsic and stacking fault pinning in the (RE)BCO system, and features in both tape and bulk data. However, the $B \parallel c$ peak is caused by strong correlated columnar pinning and is typically only observed in coated-conductors with added pinning sites such as Zr-doped (RE)BCO [76].

Figure 8 shows the $J_c(85\text{ K}, B, \theta)$ and $n(85\text{ K}, B, \theta)$ data for the TSMG GdBCO-Ag bulk. Unlike in the 77 K data shown in Figure 7a, there is no crossover between the J_c curves at different field magnitudes, which would indicate a fishtail effect. This implies that at higher T, the pinning landscape changes and the δT_c-pinning contribution becomes relatively weaker. This is further evidenced by the reduction and eventual disappearance of the second peak in $J_c(T,B)$ at increasing temperatures, as shown for the $\theta = 0°$ case in Figures 5 and 6. Therefore, it is important to measure $J_c(T,B,\theta)$ across the full region of interest if the data is to be used to simulate material behaviour.

Parameter	Bulk	HTS tape
T [K]	77	77.5
$J_c(0\text{ T}, 0°)$[A/m^2]	4.26×10^8	5.43×10^{10}
$n(0\text{ T}, 0°)$	18.0	41.6

Table 1. Self-field critical current density and flux-flow exponent of both a GdBCO-Ag bulk and a GdBCO HTS tape. Data is extracted from Figure 7.

4. Conclusions

A reliable sample preparation and mounting method has been developed which enables the transport characterisation of (RE)BCO bulk samples using transport methods for $I \leq 1.2$ kA, $|B| \leq 8$ T, $T \geq 72$ K, and arbitrary θ.

Transport $J_c(T, B_\perp)$ measurements of a TSMG

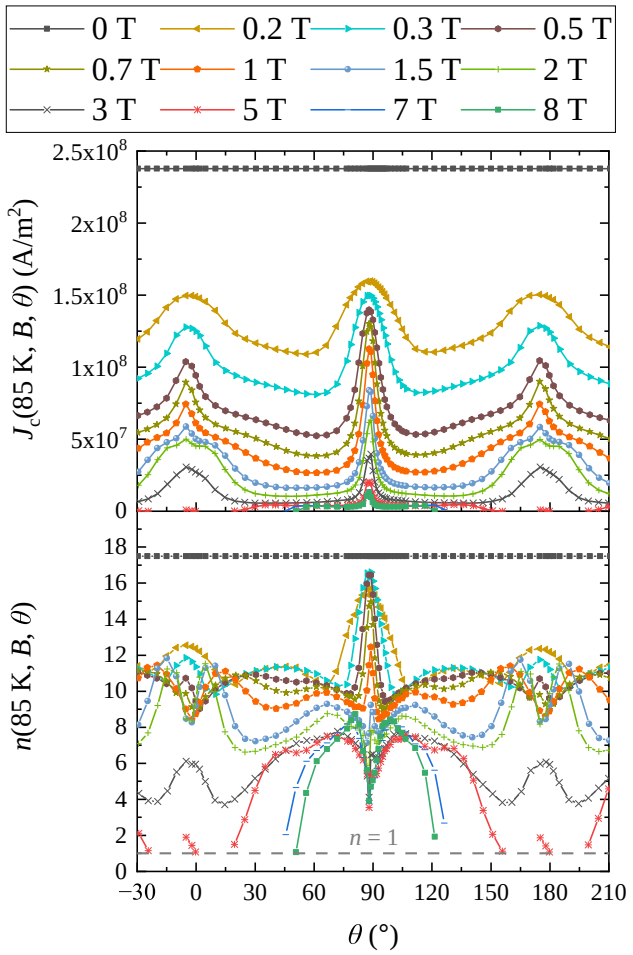

Figure 8. Transport-derived $J_c(85\ \mathrm{K}, B, \theta)$ (top) and $n(85\ \mathrm{K}, B, \theta)$ (bottom) data for TSMG GdBCO-Ag bulk Sample A.

GdBCO-Ag bulk were compared to magnetisation-derived values and found qualitatively similar. The transport J_c results were always higher than the magnetisation values, which is expected because of the different effective electric field criteria. Scaling the transport criterion from 1 µV/cm to 10^{-4} µV/cm results in good J_c agreement between methods.

Transport-derived $J_c(T, B, \theta)$ data for the TSMG GdBCO-Ag bulk were compared to equivalent data for a SuNAM SCN12700 GdBCO coated-conductor tape. The bulk and tape exhibited qualitatively different behaviour, with the tape data featuring neither a fishtail effect nor a $B \parallel c$ peak, both of which were present in the bulk data.

All J_c and n-value data presented within this manuscript are available in the *Supplementary Material*, and can be interpolated into finite-element models to more accurately capture the superconducting behaviour of GdBCO superconductors.

Acknowledgements

Financial support for this work came from NZ Marsden Grant MFP-VUW1806, and NZ Ministry of Business, Innovation and Employment's SSIF AETP contract RTVU2004. The work of T. Hlásek was supported by the Czech Science Foundation (project 24-10171S).

References

[1] Durrell J H, Ainslie M D, Zhou D, Vanderbemden P, Bradshaw T, Speller S, Filipenko M and Cardwell D A 2018 *Supercond. Sci. Technol.* **31** 103501

[2] Namburi D K, Shi Y and Cardwell D A 2021 *Supercond. Sci. Technol.* **34** 053002

[3] Sotelo G, Dias D, Motta E, Sass F, Ferreira A, de Andrade R and Stephan R 2012 *Phys. Procedia* **36** 943–947

[4] Werfel F N, Floegel-Delor U, Rothfeld R, Riedel T, Goebel B, Wippich D and Schirrmeister P 2011 *Supercond. Sci. Technol.* **25** 014007

[5] Durrell J H, Dennis A R, Jaroszynski J, Ainslie M D, Palmer K G B, Shi Y H, Campbell A M, Hull J, Strasik M, Hellstrom E E and Cardwell D A 2014 *Supercond. Sci. Technol.* **27** 082001

[6] Calvi M, Ainslie M D, Dennis A, Durrell J H, Hellmann S, Kittel C, Moseley D A, Schmidt T, Shi Y and Zhang K 2019 *Supercond. Sci. Technol.* **33** 014004

[7] Nakamura T, Itoh Y, Yoshikawa M, Oka T and Uzawa J 2007 *Concepts Magn. Reson. Part B: Magn. Reson. Eng.* **31B** 65–70

[8] Nakamura T, Tamada D, Yanagi Y, Itoh Y, Nemoto T, Utumi H and Kose K 2015 *J. Magn. Reson.* **259** 68–75

[9] Ogawa K, Nakamura T, Terada Y, Kose K and Haishi T 2011 *Appl. Phys. Lett.* **98** 234101

[10] Ainslie M and Fujishiro H 2019 *Numerical modelling of bulk superconductor magnetisation* (IOP Publishing)

[11] Salama K and Lee D F 1994 *Supercond. Sci. Technol.* **7** 177

[12] Krabbes G, Fuchs G, Schätzle P, Gruß S, Park J, Hardinghaus F, Stöver G, Hayn R, Drechsler S L and Fahr T 2000 *Phys. C: Supercond. Appl.* **330** 181–190

[13] Nariki S, Sakai N, Murakami M and Hirabayashi I 2004 *Phys. C: Supercond. Appl.* **412** 557–565

[14] Ainslie M D, Fujishiro H, Mochizuki H, Takahashi K, Shi Y H, Namburi D K, Zou J, Zhou D, Dennis A R and Cardwell D A 2016 *Supercond. Sci. Technol.* **29** 074003

[15] Shi Y, Gough M, Dennis A R, Durrell J H and Cardwell D A 2020 *Supercond. Sci. Technol.* **33** 044009

[16] Shi Y, Mousavi T, Dennis A R, Ainslie M D, Speller S C, Grovenor C R H, Durrell J H and Cardwell D A 2022 *Supercond. Sci. Technol.* **35** 105002

[17] Cayado P, Namburi D K, Erbe M, Hänisch J, Cardwell D A, Durrell J H and Holzapfel B 2023 *Appl. Phys. A* **129** 137

[18] Kuchárová V, Diko P, Volochova D, Antal V, Lojka M, Hlásek T and Plecháček V 2022 *J. Eur. Ceram. Soc.* **42** 6533–6541

[19] Shi Y, Bergamo-Andreis G, Dennis A R, Durrell J H and Cardwell D A 2020 *Supercond. Sci. Technol.* **33** 035003

[20] Kikegawa T, Sasaki H, Tada H, Kudo T, Kikuchi H, Konno K, Muralidhar M, Murakami M, Noto K, Awaji S *et al.* 2005 *Phys. C: Supercond. Appl.* **426** 649–653

[21] Vanderbemden P, Misson V, Ausloos M and Cloots R 2002 *Phys. C: Supercond. Appl.* **372** 1225–1228

[22] Chen D and Goldfarb R B 1989 *J. Appl. Phys.* **66** 2489–2500

[23] Shiohara Y and Endo A 1997 *Mater. Sci. Eng. R Rep.* **19** 1–86

[24] Fisher L, Kalinov A, Savel'ev S, Voloshin I and Yampol'skii V 1998 *Phys. C: Supercond. Appl.* **309** 284–294

[25] Yamasaki H and Mawatari Y 2000 *Supercond. Sci. Technol.* **13** 202

[26] Martinez E, Martinez-Lopez M, Millan A, Mikheenko P, Bevan A and Abell J S 2007 *IEEE Trans. Appl. Supercond.* **17** 2738–2741

[27] Vanderbemden P, Hong Z, Coombs T A, Denis S, Ausloos M, Schwartz J, Rutel I B, Hari Babu N, Cardwell D A and Campbell A M 2007 *Phys. Rev. B* **75** 174515

[28] Plummer C and Evetts J 1987 *IEEE Trans. Magn.* **23** 1179–1182

[29] Rhyner J 1993 *Phys. C: Supercond. Appl.* **212** 292–300

[30] Miyamoto T, Nagashima K, Sakai N and Murakami M 2000 *Supercond. Sci. Technol.* **13** 816

[31] Chunlin J, Zhanguo F, Guofan Z, Guiyi Z, Weimin B, Zhongxian Z and Shuquan G 1991 *Supercond. Sci. Technol.* **4** 49

[32] Selvamanickam V, Forster K and Salama K 1991 *Phys. C: Supercond. Appl.* **178** 147–157

[33] Ekin J, Salama K and Selvamanickam V 1991 *Appl. Phys. Lett.* **59** 360–362

[34] Ekin J 1992 *Cryogenics* **32** 1089–1091

[35] Lee D, Selvamanickam V and Salama K 1992 *Phys. C: Supercond. Appl.* **202** 83–96

[36] Braithwaite D, Bourgault D, Schopohl N, Tournier R, Barbut J and Vallier J 1993 *J. Low Temp. Phys.* **92** 295–305

[37] Porcar L, Bourgault D, Barbut J, Chaud X and Tournier R 1998 *Cryogenics* **38** 1237–1242

[38] Rush J, May-Miller C, Palmer K, Rutter N, Dennis A, Shi Y H, Cardwell D and Durrell J 2016 *IEEE Trans. Appl. Supercond.* **26** 6800904

[39] Taylor R W, Pantoja A E, Hlásek T, Plecháček J, Weijers H W, Ainslie M D and Bumby C W 2023 *IEEE Trans. Appl. Supercond.* **33** 6800106

[40] Taylor R W, Weijers H W, Ainslie M D, Congreve J V J, Durrell J H, Badcock R A and Bumby C W 2024 *Supercond. Sci. Technol.* **37** 03LT01

[41] Antončík F, Lojka M, Hlásek T, Plecháček V and Jankovský O 2022 *Ceram. Int.* **48** 5377–5385

[42] Strickland N M, Hoffmann C and Wimbush S C 2014 *Rev. Sci. Instrum.* **85** 113907

[43] Strickland N M, Wimbush S C, Pantoja A, Pooke D M, Fee M, Chamritskii V, Hartwig Z, Cheng J, Garberg S, and Sorbom B 2021 *IEEE Trans. Appl. Supercond.* **31** 9000305

[44] Wimbush S C 2020 *Targeted Selection and Characterisation of Contemporary HTS Wires for Specific Applications* (Cham.: Superconductivity. Springer)

[45] Sun Y, Fang J, Pantoja A E, Badcock R A, Long N J and Jiang Z 2021 *J. Appl. Phys.* **130** 083902

[46] Wimbush S C and Strickland N M 2022 *Supercond. Sci. Technol.* **35** 024004

[47] Jiang Z, Endo N, Wimbush S C, Brooks J, Song W, Badcock R A, Miyagi D and Tsuda M 2019 *J. Phys. Commun.* **5** 095017

[48] Brooks J M, Ainslie M D, Jiang Z, Pantoja A E, Badcock R A and Bumby C W 2020 *Supercond. Sci. Technol.* **33** 035007

[49] Wimbush S C and Strickland N M 2017 *IEEE Trans. Appl. Supercond.* **27** 8000105

[50] Molodyk A, Samoilenkov S, Markelov A, Degtyarenko P, Lee S, Petrykin V, Gaifullin M, Mankevich A, Vavilov A, Sorbom B, Cheng J, Garberg S, Kesler L, Hartwig Z, Gavrilkin S, Tsvetkov A, Okada T, Awaji S, Abraimov D, Francis A, Bradford G, Larbalestier D, Senatore C, Bonura M, Pantoja A E, Wimbush S C, Strickland N M and Vasiliev A 2021 *Sci. Rep.* **11** 2084

[51] Wimbush S C, Strickland N M and Long N J 2015 *IEEE Trans. Appl. Supercond.* **25** 6400105

[52] Weber H W 2005 Flux pinning *Handbook on the Physics and Chemistry of Rare Earths* vol 34 ed Karl A Gschneidner J C G B and Pecharsky V K (Elsevier) chap 196, pp 187–243

[53] Namburi D K, Shi Y and Cardwell D A 2021 *Supercond. Sci. Technol.* **34** 053002

[54] Koblischka M and Murakami M 2000 *Supercond. Sci. Technol.* **13** 738

[55] Koblischka M, Koblischka-Veneva A and Murakami M 2004 *J. Supercond.* **17** 373–377

[56] Werner M, Sauerzopf F M, Weber H W and Wisniewski A 2000 *Phys. Rev. B* **61** 14795–14803

[57] Daeumling M, Seuntjens J and Larbalestier D 1990 *Nature* **346** 332–335

[58] Jirsa M, Pust L, Dlouhỳ D and Koblischka M 1997 *Phys. Rev. B* **55** 3276

[59] Hillmann H 1999 *Supercond. Sci. Technol.* **12** 348

[60] Blamire M 1987 *J. Low Temp. Phys.* **68** 335–352

[61] Petermann J 1970 *Int. J. Mater. Res.* **61** 724–733

[62] Willa R, Koshelev A E, Sadovskyy I A and Glatz A 2017 *Supercond. Sci. Technol.* **31** 014001

[63] Meier-Hirmer R, Küpfer H and Scheurer H 1985 *Phys. Rev. B* **31** 183

[64] van Dalen A, Koblischka M, Griessen R, Jirsa M and Ravi Kumar G 1995 *Phys. C: Supercond. Appl.* **250** 265–274

[65] Abulafia Y, Shaulov A, Wolfus Y, Prozorov R, Burlachkov L, Yeshurun Y, Majer D, Zeldov E, Wühl H, Geshkenbein V B and Vinokur V M 1996 *Phys. Rev. Lett.* **77**(8) 1596–1599

[66] Cohen L, Laverty J, Perkins G, Caplin A and Assmus W 1993 *Cryogenics* **33** 352–356

[67] Yeshurun Y, Bontemps N, Burlachkov L and Kapitulnik A 1994 *Phys. Rev. B* **49** 1548–1551

[68] Zhukov A A, Küpfer H, Claus H, Wühl H, Kläser M and Müller-Vogt G 1995 *Phys. Rev. B* **52** R9871–R9874

[69] Ainslie M D, Huang K Y, Fujishiro H, Chaddock J, Takahashi K, Namba S, Cardwell D A and Durrell J H 2019 *Supercond. Sci. Technol.* **32** 034002

[70] Quéval L, Liu K, Yang W, Zermeño V M R and Ma G 2018 *Supercond. Sci. Technol.* **31** 084001

[71] Ainslie M D, Fujishiro H, Ujiie T, Zou J, Dennis A R, Shi Y H and Cardwell D A 2014 *Supercond. Sci. Technol.* **27** 065008

[72] Yeshurun Y, Malozemoff A P and Shaulov A 1996 *Rev. Mod. Phys.* **68**(3) 911–949

[73] Caplin A D, Cohen L F, Perkins G K and Zhukov A A 1994 *Supercond. Sci. Technol.* **7** 412

[74] Taylor R, Booth T, Ainslie M, Weijers H, Badcock R and Bumby C 2022 *Superconductivity* **4** 100026

[75] Zermeño V M R, Habelok K, Stepień M and Grilli F 2017 *Supercond. Sci. Technol.* **30** 034001

[76] Xu A, Delgado L, Khatri N, Liu Y, Selvamanickam V, Abraimov D, Jaroszynski J, Kametani F and Larbalestier D C 2014 *APL Mater.* **2** 046111